NON-PROPORTIONALITY OF STRAIN AND COUPLING EFFECTS ON DISLOCATION DISTRIBUTION AND DUCTILITY IN FERRITIC STEEL POLYCRYSTALS

T.O ERINOSHO*, A.C.F COCKS† AND F.P.E DUNNE*

* Department of Materials
Imperial College London
South Kensington, SW7 2AZ, London, United Kingdom

† Department of Engineering Science
University of Oxford
Parks Road, OX1 3PJ, Oxford, United Kingdom

Abstract. Non-proportionality of straining, initial texture and hardening have been investigated in a ferritic steel polycrystal within a crystal plasticity finite element framework. Two extreme forms of hardening are investigated; namely, isotropic latent-hardening and anisotropic self-hardening. Dislocation density evolutions on all independent slip systems have been calculated in order to investigate the establishment of dislocation distributions and evaluate their dependence on non-proportionality, hardening, texture and predicted ductility. The results show that non-proportionality effects are more pronounced under isotropic latent-hardening as opposed to anisotropic self-hardening especially under non-proportional uniaxial strains.

Key words: Non-proportionality, texture, hardening, dislocation distributions, forming limits, necking, strain localization

1. Introduction

This paper provides an overview on the effects of non-proportionality of strain, its link with texture, dislocation distributions and their consequent effects on predicted ductility in ferritic steel polycrystals within a crystal plasticity finite element framework. Two initial textures are incorporated within a polycrystal and investigated under two hardening forms (anisotropic self- and isotropic latent-hardening). The formation of dislocation distributions under non-proportional strain paths is evaluated and in addition, ductility is predicted using a proposed failure criterion for various non-proportional strain paths. The motivation for this study lies in further understanding the mechanisms that drive non-proportionality effects in ferritic steel.

Sheet processing is an important stage in the manufacturing of automobiles. Ideally, strains are applied to sheets within an established strain safe region commonly described by a forming limit diagram (FLD) [1]. The limit diagram represents a safety curve above which the material is considered necked a below which, safe straining is assumed. Empirical evidence suggests that subjecting metals to a non-proportional strain path enables higher levels of strain to be achieved. Conversely, premature failure may also occur when a counter-beneficial strain path is employed. Limit strains are obtained experimentally by using a hemispherical punch-stretching test on carefully marked flat metal sheets until the onset of necking is observed. However, due to associated costs, FLDs are predicted computationally by evaluating the onset of strain instabilities within the material on the basis of localization criteria.

Numerous techniques have been reported and implemented to predict limit strains within phenomenological and crystal plasticity frameworks [2-4], [5], [6] [7-10]. However, these studies have centered on predicting FLDs under proportional strains and have not investigated the effects of strain non-proportionality on ductility in the context of hardening, and texture. Similarly, studies on dislocation structures in polycrystals undertaken within phenomenological and crystal plasticity frameworks also lack information in predicting response to non-proportional strains [11-14].

In this paper, two hardening models are investigated; self- and isotropic latent-hardening models adopted from [15]. A failure criterion implemented within a crystal plasticity framework is coupled with these hardening models and a representative oligocrystal is used to investigate the response of ferritic steel to non-proportional strain paths. The development of dislocation distributions is shown and the effect of texture on predicted ductility in ferritic steel is presented.

2. Crystal plasticity framework, hardening model and dislocation distributions

The crystal plasticity framework used here is based on the kinematic decomposition of the deformation gradient into elastic ($\boldsymbol{F}^{*}$) and plastic ($\boldsymbol{F}^{\mathrm{p}}$) tensors laid out by [16] and implemented into a VUMAT (see [17] for an overview).

2.1. Hardening model and dislocation distributions

On the basis that non-proportionality effects in polycrystals result from the formation of dislocation distributions that are strain path dependent, dislocation evolution on slip systems in the polycrystal is tracked within a crystal plasticity framework. Dislocations are calculated based on the hardening developed on each slip system. The hardening law adopted by [15] and others [7] and [8] has been employed in this study. Consider the slip system strength g, also indicative of the resistance to dislocation motion calculated such that the hardening modulus h_0, and fitting parameter, m are determined for a particular BCC steel being investigated. Hence, the strength on each slip system is calculated using

$$\dot{g}^{\alpha} = h_0 \left(1 + \frac{h_0 \gamma_{\mathrm{sum}}}{\tau_0 m}\right)^{m-1} \dot{\gamma}^{\alpha} \tag{1}$$

where the accumulated slip is given by

$$\gamma_{\mathrm{sum}} = \sum_{\beta=1}^{N_{\mathrm{slip}}} \left(\int_0^{\mathrm{t}} \dot{\gamma} \, dt \right) \tag{2}$$

and dislocation densities on active slip systems are updated according to

$$\rho^{\alpha} = \int_0^t \dot{\rho}^{\alpha} dt \,. \tag{3}$$

The physical relationship between slip system strength and dislocation density is given by

$$g^{\alpha} = g_0 + \beta \sqrt{\rho^{\alpha}} \,. \tag{4}$$

where the density of dislocations on each slip system is calculated based on an initial value of strength for a particular slip system and updated based on eqs. (1) – (4). The two forms of

hardening considered here are isotropic latent-hardening and anisotropic self-hardening. Under isotropic latent-hardening, active slip systems cause hardening on the inactive systems.

$$\dot{g} = h_0(1+\frac{h_0\gamma_{\text{sum}}}{\tau_0 m})^{m-1}(\dot{\gamma})_{\max}. \tag{5}$$

A second possible form is termed self-hardening. In this case, the slip resistance only develops on active slip systems and dislocation densities are calculated based on these active systems.

$$\dot{g}^{\alpha} = h_0(1+\frac{h_0\gamma_{\text{sum}}}{\tau_0 m})^{m-1}\dot{\gamma}^{\alpha}. \tag{6}$$

The behavioral trend observed experimentally shows that mixed forms of hardening typically develop in polycrystals. However, implementing these two forms of hardening (anisotropic self- and isotropic latent) provide an insight into dislocation responses as well as failure prediction in ferritic steel polycrystals. Another form of hardening not investigated here is a form of latent hardening in which hardening on active slip systems result in more hardening on the inactive systems. Investigations have shown that the predicted response is similar to isotropic latent-hardening adopted here [18]. Also, the authors are aware of more advanced dislocation models to predict dislocation evolution on slip systems [19]. However, this simple phenomenological model has been adopted in this paper for investigatory purposes prior to implementing more advanced dislocation models.

Dislocation distributions

The investigation of dislocation distributions formed upon straining a polycrystal provides a basis for justifying the effects of non-proportionally straining BCC polycrystals. Apart from texture which also accounts for non-proportionality effects (usually in the form of higher or lower ductility), the possibility of evaluating dislocation distributions provides an insight into potential strain paths that will exhibit clear differences in terms predicted ductility. Since all the straining is applied in the 1-2 plane, the distributions are generated by rotating all slip directions in each grain of the polycrystal into the 1-2 plane and averaging dislocation densities, binned based on the angle θ between the rotated slip vector and the [100] direction such that

$$\rho_{\theta}^{\text{avg}} = \frac{\rho_{\theta}^{\text{tot}}}{N_{\theta}} = \sum_{\beta=1}^{N_{\text{grains}}}\sum_{\alpha=1}^{N_{slip}}\rho_{\theta}^{\alpha}. \tag{7}$$

N_{grains} and N_{slip} represent the number of grains in the oligocrystal and the number of slip directions in each grain respectively and $\rho_{\theta}^{\text{avg}}$ denotes the average density of dislocations of orientation θ based on the summation of binned slip direction densities $\rho_{\theta}^{\text{tot}}$ and the total number of slip directions within each grain that fall within the cutoff criterion of 1 degree, N_{θ}.

2.2. Material properties

The material properties used in the slip rule and hardening model have been determined for a ferritic steel using a representative volume element with 216 randomly

oriented grains under uniaxial loading conditions, illustrated in Fig. 1a. The yield strength and isotropic hardening properties were chosen in order for the macroscopic stress-strain response from the polycrystal shown in Fig. 1b to match experimental observations for the ferritic steel considered. Furthermore, strain rate effects have been neglected since they are likely to be negligible at room temperature for ferritic steel and the rate sensitivity parameter, n, in the slip rule has been chosen appropriately for this purpose. The macro-mechanical properties for the ferritic steel being considered and the material properties used in the simulations are given in Table 1.

2.3. Body centered cubic system (BCC) slip

The twelve slip systems, {110}<111>, present in BCC crystals have been incorporated into an ABAQUS user material subroutine and used in all simulations. It has been shown that texture and stress response in BCC metals can be adequately predicted using the {110}<111> set of slip systems [20, 21]. An earlier study by [22] on dislocation evolution in Niobium crystals investigated the relative roles of the BCC slip system families and concluded that using the first 24 slip system families provided the closest agreement to experimental data. It can however be drawn from that study that the error associated with the prediction using the first 12 slip systems is moderate. Hence, due to the numerous number of simulations to be undertaken in this paper and for computational efficiency, the full 48 slip systems, which consist of {112}<111> and {123}<111> slip systems in addition to the {110}<111> slip systems have not been accounted for in this present work.

3. 3-D model development, localization criterion and measure of non-proportionality

This section outlines a description of the models adopted in this study. Further, the initial textures used in this paper are shown, boundary conditions are outlined, the localization criterion adopted is validated and non-proportional strain paths are illustrated.

3.1. 3-D model development

The model adopted in this paper has 216 grains, each grain consisting of 3×3×3 C3D8R elements shown in Fig. 2. In all simulations, displacement is applied to the in-plane surfaces (positive 1- and 2- surfaces), and the back surfaces are constrained to remain planar. Also, the positive 3- surface is constrained to remain planar.

3.2. Initial texture

Two textures are adopted in this paper. An initially randomly oriented texture (R-1) has been investigated as shown by the pole figures in Fig. 3a and a measured ferritic steel (FS-1) texture is also evaluated (Fig. 3b). Texture R-1, computationally generated, gives a general insight into material behavior while FS-1, shows the effects of directionality typically present in rolled sheet metals.

3.3. Localization criterion

The onset of necking is determined by evaluating local critical grains developing plastic strains in the polycrystal model based on the increments of plastic strain between t_n and t_{n+1}, normalized with respect to the macro plastic strain increment within the

corresponding deformation states. This criterion is similar to the combined approach adopted by Volk and Hora [9] in which the onset of instabilities within a polycrystal is evaluated by tracking plastic strain increments during a deformation history on the basis of experimental knowledge of fracture point. The failure criterion utilized here is fully outlined and calibrated in [23].

Validation of failure criterion under proportional strain paths

The forming limit curve under proportional strain paths has been predicted by subjecting the polycrystal in Fig. 2a to a range of proportional strain paths. These proportional strain paths (A-E) shown in Fig. 4a were applied to the positive 1- and 2- surfaces of the polycrystal and the onset of localization along each path based on the normalized, incremental average plastic strain is indicated in Fig. 4b. The predicted limit strain curve for the Numisheet 2008 BM 1 ferritic steel [24] is compared to its experimentally obtained response [9]. As seen in Fig. 4b, a close agreement is observed and on this basis, the failure criterion will be used to predict limit strain under non-proportional strain paths.

.

3.4. Non-proportional strain paths adopted

The primary purpose of this paper is to investigate the response of ferritic steel polycrystals to non-proportional strain paths such as that shown in Fig. 5. The notation is such that proportional biaxial and uniaxial strain paths are represented by B-1 and U-1 respectively. Both proportional strain paths are encompassed by a range of non-proportional paths consisting of two stages. Consider path B-2 which represents a non-proportional biaxial strain path and consists of B-2a and B-2b that terminate at a biaxial state (B). Similarly, U-5 represents a non-proportional uniaxial strain consisting of plane strain tension followed by a plane strain compression to a final uniaxial state (U).

The positive 1- and 2- surfaces of the polycrystal in Fig. 2 have been subjected to the individual strain paths in Fig. 5 and the results are discussed next.

4. Effects of texture, hardening and non-proportionality on limit strain in BCC polycrystals

The coupled effects of non-proportionality, texture and hardening on predicted ductility is discussed in this section. Firstly, formed dislocation distributions based on the slip system binning methodology outlined earlier is shown schematically for non-proportional biaxial strain paths on the basis of anisotropic self-hardening. Subsequently, the distributions are shown graphically in more details for both cases of hardening- anisotropic self- and isotropic latent-hardening. And finally, the effects of non-proportionality on predicted ductility are presented on the basis of a failure criterion fully outlined in [23].

The term dislocation distributions and its link with non-proportionality is a concept used continuously throughout this paper. Since dislocation evolution is accounted for on each slip system within the crystal plasticity framework, it is possible to classify similarly oriented slip systems within a polycrystal and to schematically show the density of dislocations. On the basis of the dislocation binning methodology outlined in the previous section, similarly oriented slip systems are shown in Fig. 6 for a through section of a polycrystal subjected to proportional and non-proportional biaxial strain B-1 and B-4 respectively (illustrated in Fig. 5). Note that B-1 represents proportional biaxial strains while B-4 consists of consecutive

plane strain phases in the 1- and 2- directions to achieve a final biaxial state. A cutoff criterion of 10 degrees has been adopted in Fig. 6 and the strain-path based distribution of dislocation within the polycrystal is shown for angular ranges between 0^0 and 180^0. It is clear that different dislocation distributions result within the polycrystal at the final biaxial state. Although, evaluating the effects of these distributions on non-proportionality behavior remains unclear, it is worth investigating since it can provide insight into particular observed responses. To provide a clearer overview on strain-path based response to non-proportional strains, the average binned dislocation density on similarly oriented slip systems throughout the polycrystal will be subsequently shown graphically.

Fig. 7 illustrates the dislocation distribution for non-proportional biaxial strain under anisotropic self- and isotropic latent-hardening. Consider Fig. 7a which shows dislocation distribution responses for texture R-1 at the final biaxial state for non-proportional strain paths B-1, B-3 and B-4, it is seen that the dislocation distribution response to the various strain paths are similar. However, in comparison with Fig. 7b, clearer differences in response are seen even at an identical biaxial state and at considerably low strains (25%). Consider the initially textured polycrystal denoted by FS-1, a similar response is observed under both forms of hardening, but a significantly higher dispersion is observed at higher angles under isotropic latent-hardening.

Fig. 8 shows the dislocation distribution responses for textures R-1 and FS-1 at a final uniaxial state for strain proportional strain path U-1 and a range of non-proportional paths U-3, U-4 and U-5 (illustrated in Fig. 5). Consider Fig. 8a and 8b in which the response of the polycrystal with initially random texture R-1 is shown for the case of anisotropic self- and isotropic latent-hardening respectively. The differences in dislocation distributions are clearly seen for the range of non-proportional paths under isotropic latent-hardening as opposed to anisotropic self-hardening. This can also be observed in Fig. 8c and 8d for ferritic steel texture FS-1 under both hardening forms respectively.

By comparing the dislocation distribution responses to biaxial and uniaxial strain paths, it is clear that the effects of non-proportionality are more visible under uniaxial strain paths and more so, under isotropic latent-hardening. The symmetry associated with biaxial strain arguably results in less pronounced differences in dislocation distributions at the final biaxial state. But, it is imperative to investigate ductility and evaluate the effects of non-proportionality. An important question that arises is whether larger differences in ductility are achievable under non-proportional uniaxial strains as against biaxial strains on the basis of the formed dislocation distributions.

The ductility (based on the average plastic strain in the polycrystal) under non-proportional strain paths are shown below for textures R-1 and FS-1 under both forms of hardening. Consider Fig. 9a and 9b which shows the predicted ductility for both initial textures under isotropic latent-hardening and anisotropic self-hardening respectively. Here, minor deviations from proportionality indicated by non-proportional paths B-3 and U-3 previously illustrated in Fig. 5 are compared with their corresponding proportional strains B-1 and U-1.

In both hardening cases, clear differences are observed under non-proportional uniaxial strain paths as opposed to biaxial strains for minor deviations from proportionality. However, consider Fig. 9a in which the predicted ductility is shown for both textures for strain paths B-1 and B-3. It can be clearly seen that the ductility achieved by ferritic steel texture FS-1 is higher than the initially random texture R-1 under proportional biaxial strains.

In addition, an increase in ductility is achieved by subjecting texture FS-1 to non-proportional strain path B-3 as against the moderate change observed in texture R-1. It is therefore plausible to argue that texture affects achievable ductility under non-proportional paths and there exists a possibility of designing a suitable starting texture in addition to a favorable strain path in order to achieve higher ductility.

5. Conclusions

The effects of straining ferritic steel polycrystals under non-proportional paths have been investigated within a crystal plasticity finite element framework incorporating a hardening law to impose isotropic latent-hardening and (anisotropic) self-hardening respectively. Systematic studies have also been carried out for polycrystal aggregates in order to investigate the effects of initial texture in combination with non-proportionality. Also, ductility under non-proportional strain paths has been predicted. The results show that;

- The differences in dislocation distributions formed under isotropic latent-hardening are more pronounced in comparison to anisotropic self-hardening for non-proportional biaxial strain paths and similarly for uniaxial strains.
- Non-proportionality, texture and the nature of the hardening affect the predicted limit strain and increases in ductility are more apparent under non-proportional uniaxial strain paths as opposed to biaxial paths (evident from the predicted dislocation distributions).

References

[1] B. Keeler, Trans.ASM, 56 (1963) 25-35.
[2] K. Yoshida, T. Kuwabara, M. Kuroda, International Journal of Plasticity, 23 (2007) 361-384.
[3] T. Kuwabara, K. Yoshida, K. Narihara, S. Takahashi, International Journal of Plasticity, 21 (2005) 101-117.
[4] J. Betten, M. Waniewski, Forschung Im Ingenieurwesen-Engineering Research, 64 (1998) 231-244.
[5] Z. Marciniak, K. Kuczynski, International Journal of Mechanical Sciences, 9 (1967) 609-620.
[6] Q. Situ, M.K. Jain, D.R. Metzger, International Journal of Mechanical Sciences, 53 (2011) 707-719.
[7] J.W. Signorelli, M.A. Bertinetti, P.A. Turner, International Journal of Plasticity, 25 (2009) 1-25.
[8] M.J. Serenelli, M.A. Bertinetti, J.W. Signorelli, International Journal of Solids and Structures, 48 (2010) 1109-1119.
[9] W. Volk, P. Hora, International Journal of Material Forming, 4 (2011) 339-346.
[10] K. Yoshida, M. Kuroda, 8th International Conference and Workshop on Numerical Simulation of 3d Sheet Metal Forming Processes (Numisheet 2011), Pts a and B, 1383 (2011) 158-164.
[11] M. Kraska, M. Doig, D. Tikhomirov, D. Raabe, F. Roters, Computational Materials Science, 46 (2009) 383-392.
[12] D. Raabe, P. Klose, B. Engl, K.P. Imlau, F. Friedel, F. Roters, Advanced Engineering Materials, 4 (2002) 169-180.
[13] I. Tikhovskiy, D. Raabe, F. Roters, Materials Science and Engineering a-Structural Materials Properties Microstructure and Processing, 488 (2008) 482-490.
[14] Y.S. Choi, M.A. Groeber, T.J. Turner, D.M. Dimiduk, C. Woodward, M.D. Uchic, T.A. Parthasarathy, Materials Science and Engineering a-Structural Materials Properties Microstructure and Processing, 553 (2012) 37-44.
[15] R.D. McGinty, D.L. McDowell, Journal of Engineering Materials and Technology-Transactions of the Asme, 126 (2004) 285-291.
[16] E.H. Lee, Journal of Applied Mechanics, 36 (1969) 1-&.
[17] F.J. Harewood, P.E. McHugh, Computational Materials Science, 39 (2007) 481-494.
[18] T. Erinosho, A. Cocks, F. Dunne, Internal Report, (2012).
[19] F. Roters, P. Eisenlohr, L. Hantcherli, D.D. Tjahjanto, T.R. Bieler, D. Raabe, Acta Materialia, 58 (2010) 1152-1211.
[20] A.C. Lewis, S.M. Qidwai, A.B. Geltmacher, Metallurgical and Materials Transactions a-Physical Metallurgy and Materials Science, 41A (2010) 2522-2531.

[21] D. Canadinc, H. Sehitoglu, H.J. Maier, P. Kurath, Materials Science and Engineering a-Structural Materials Properties Microstructure and Processing, 485 (2008) 258-271.
[22] A. Ma, F. Roters, D. Raabe, Computational Materials Science, 39 (2007) 91-95.
[23] T. Erinosho, A. Cocks, F. Dunne, Internal Report, (2013).
[24] W. Volk, R. Illig, H. Kupfer, A. Wahlen, P. Hora, Lutz, Kessler, W. Hotz, (2008).

Table 1 Material properties of ferritic steel obtained from experiment and used to fit simulation parameters

Experiment		**Simulation parameters**			
Yield strength	150 MPa	ρ_0	10^{10}m^{-2}	E	211GPa
Tensile strength	380 MPa	n	50	ν	0.3
Elastic modulus	211GPa	$\dot{\gamma}_0$	1s^{-1}	τ_0	70MPa
		m	0.245	h_0	0.9GPa

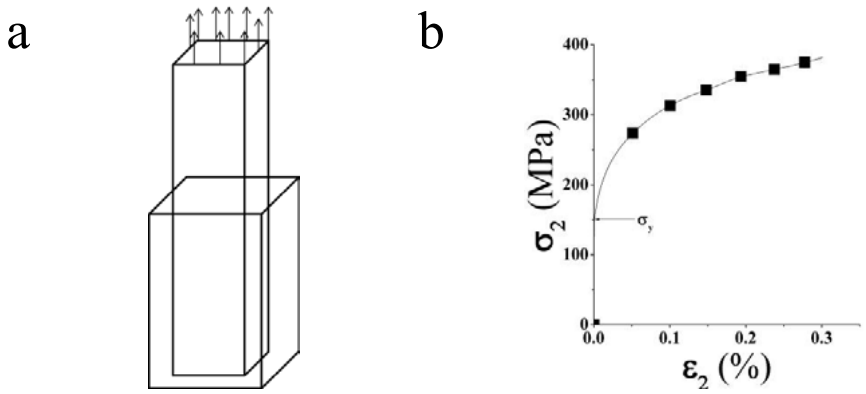

Fig. 1. Systematic determination of material properties (a) uniaxial loading on RVE (b) averaged RVE stress-strain response to determine yield strength σ_y

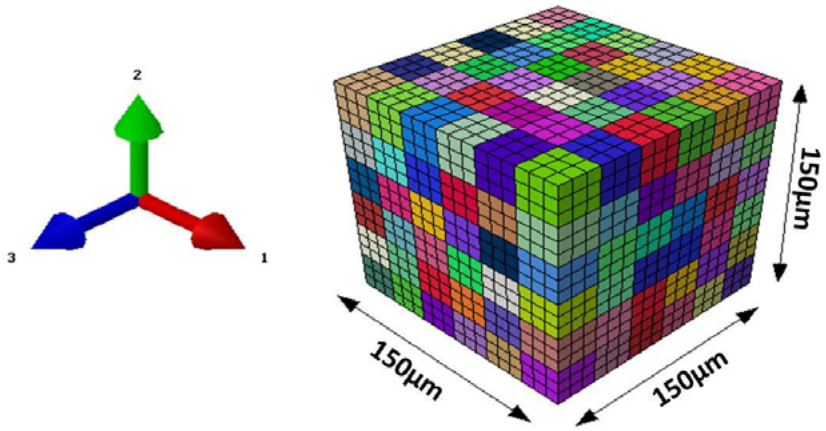

Fig. 2. The oligocrystal used in the simulations (showing 216 grains).The negative 1-, 2- and 3- surfaces are always constrained such that displacements in these directions are zero. Strain paths shown in Fig. 2 are applied to the positive 1- and 2- surfaces.

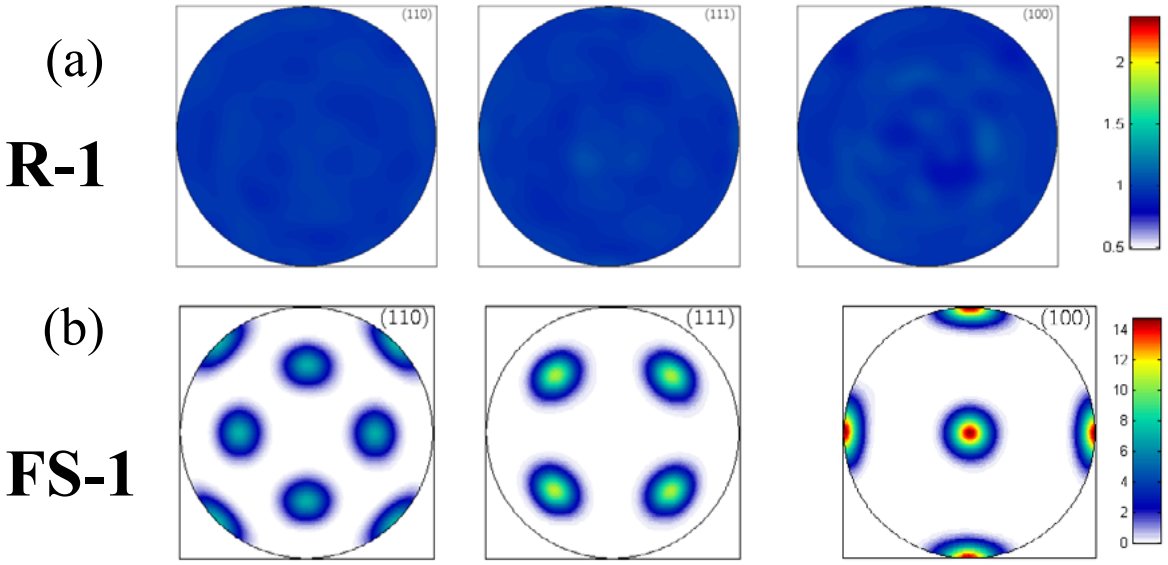

Fig. 3. Pole figures showing the initial textures used in the simulations (a) R-1: random texture and (b) FS-1: ferritic steel texture

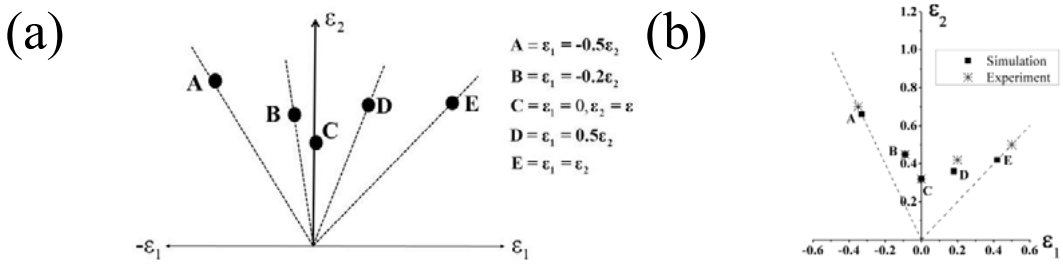

Fig. 4. Prediction of limit strain (a) schematic of proportional strain paths used to validate the failure criterion (b) comparison of limit strains predicted using the computational model as against experimental results from Volk and Hora [9]

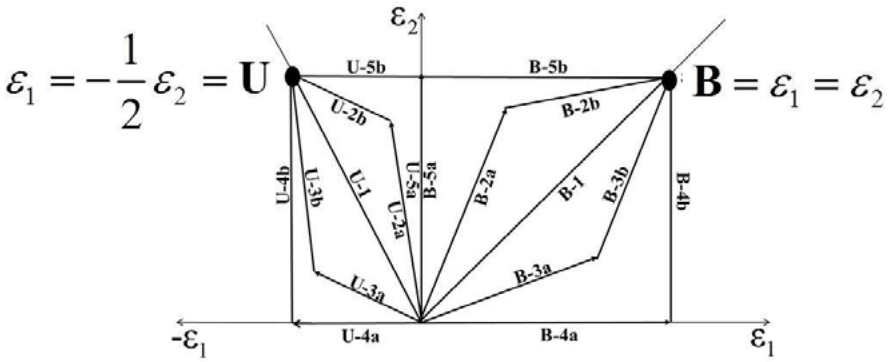

Fig. 5. Displacement controlled non-proportional strain paths

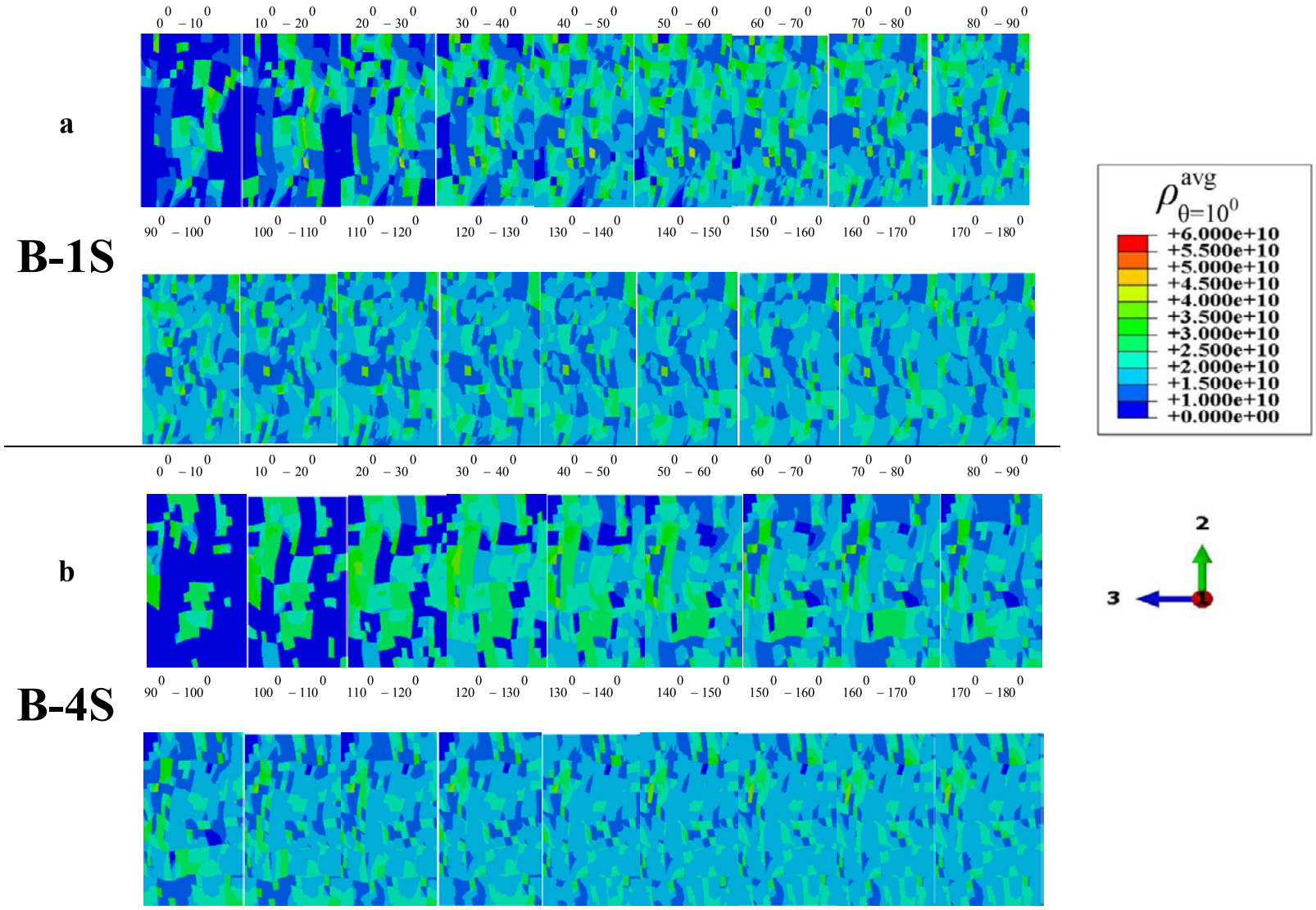

Fig. 6 Schematic representation of dislocation distribution for texture R-1 subjected to non-proportional strain paths to biaxial tension state. Note that the angle ranges indicate dislocation densities on similarly oriented slip systems within the polycrystal binned at 10 degree intervals.

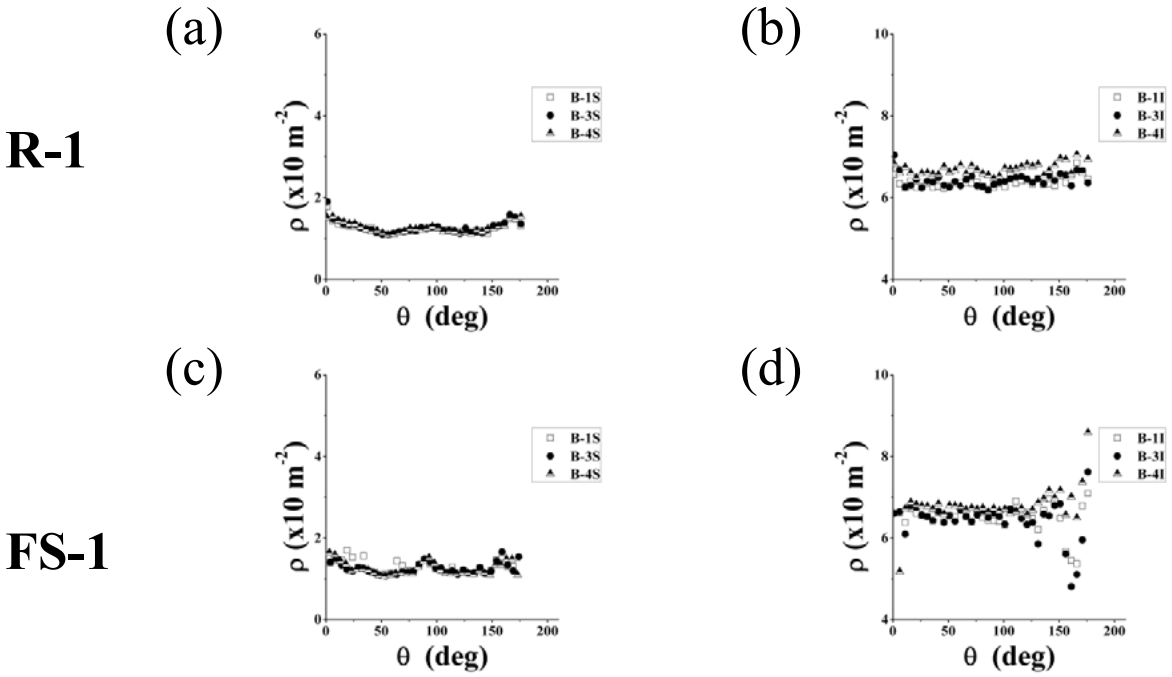

Fig. 7 Dislocation distribution for textures R-1 and FS-1 under non-proportional strain paths to biaxial tension state. (a) dislocation distribution for R-1 at biaxial state under anisotropic self-hardening, (b) dislocation distribution of R-1 at final biaxial tension state under isotropic latent hardening (c) dislocation distribution for FS-1 at biaxial state under anisotropic self-hardening, (b) dislocation distribution of FS-1 at final biaxial tension state under isotropic latent hardening.

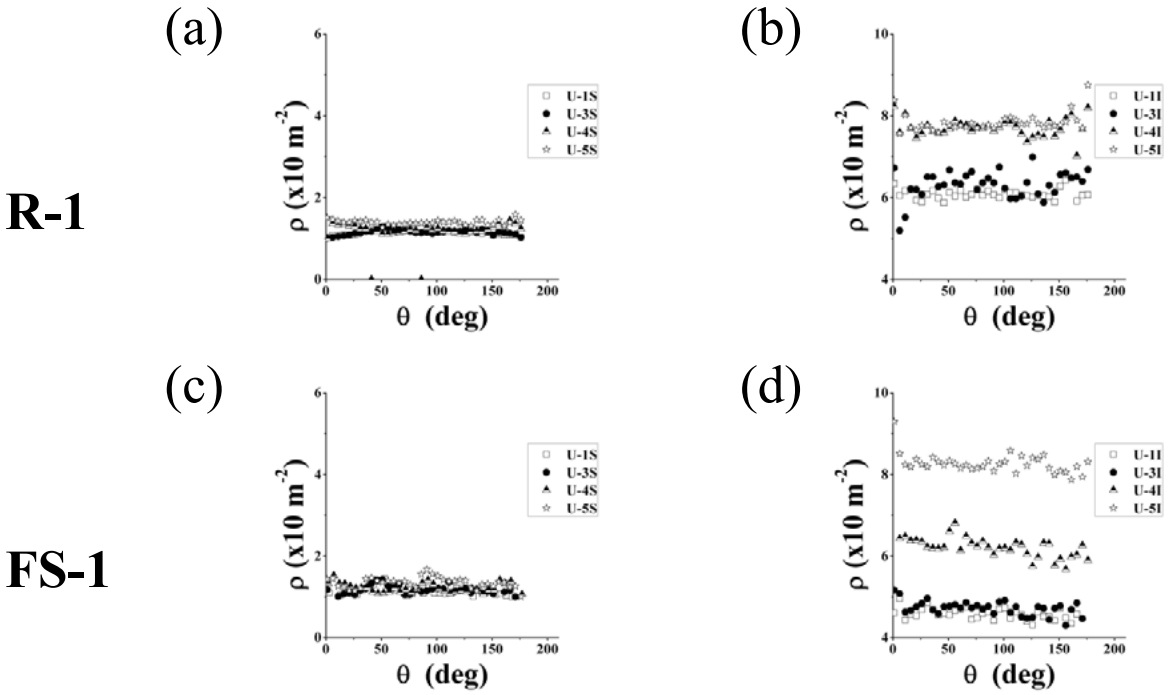

Fig. 8 Dislocation distribution for textures R-1 and FS-1 under non-proportional strain paths to uniaxial tension state. (a) dislocation distribution for R-1 at uniaxial state under anisotropic self-hardening, (b) dislocation distribution of R-1 at final uniaxial tension state under isotropic latent hardening (c) dislocation distribution for FS-1 at uniaxial state under anisotropic self-hardening, (b) dislocation distribution of FS-1 at final uniaxial tension state under isotropic latent hardening.

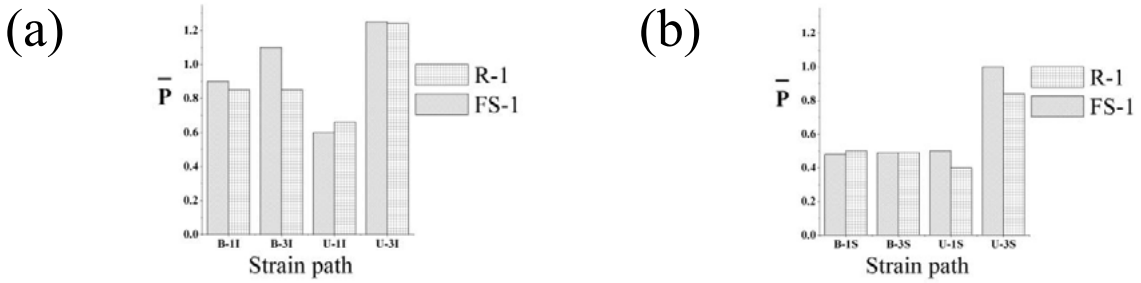

Fig. 9. Comparison of predicted ductility achieved under proportional biaxial (B-1) and uniaxial (U-1) strain paths as against the non-proportional cases indicated by B-3 and U-3 respectively. (a) under isotropic latent-hardening (b) anistropic self-hardening